AGU PUBLICATIONS

JGR

Journal of Geophysical Research: Atmospheres

RESEARCH ARTICLE
10.1002/2014JD021665

Key Points:
- A stochastic model for multiple BC/dust internal inclusions in snow is developed
- Absorption and scattering properties are computed by improved photon tracing
- Two-layer snow model with fresh snow on top of old snow is developed for climate

Correspondence to:
Y. Takano,
ytakano@atmos.ucla.edu

Citation:
Liou, K. N., Y. Takano, C. He, P. Yang, L. R. Leung, Y. Gu, and W. L. Lee (2014), Stochastic parameterization for light absorption by internally mixed BC/dust in snow grains for application to climate models, *J. Geophys. Res. Atmos.*, *119*, 7616–7632, doi:10.1002/2014JD021665.

Received 18 FEB 2014
Accepted 28 MAY 2014
Accepted article online 2 JUN 2014
Published online 26 JUN 2014

Stochastic parameterization for light absorption by internally mixed BC/dust in snow grains for application to climate models

K. N. Liou[1], Y. Takano[1], C. He[1], P. Yang[2], L. R. Leung[3], Y. Gu[1], and W. L. Lee[4]

[1]Joint Institute for Regional Earth System Science and Engineering, and Department of Atmospheric and Oceanic Sciences, University of California, Los Angeles, California, USA, [2]Department of Atmospheric Sciences, Texas A&M University, College Station, Texas, USA, [3]Pacific Northwest National Laboratory, Richland, Washington, USA, [4]Research Center for Environmental Changes, Academia Sinica, Taipei, Taiwan

Abstract A stochastic approach has been developed to model the positions of BC (black carbon)/dust internally mixed with two snow grain types: hexagonal plate/column (convex) and Koch snowflake (concave). Subsequently, light absorption and scattering analysis can be followed by means of an improved geometric-optics approach coupled with Monte Carlo photon tracing to determine BC/dust single-scattering properties. For a given shape (plate, Koch snowflake, spheroid, or sphere), the action of internal mixing absorbs substantially more light than external mixing. The snow grain shape effect on absorption is relatively small, but its effect on asymmetry factor is substantial. Due to a greater probability of intercepting photons, multiple inclusions of BC/dust exhibit a larger absorption than an equal-volume single inclusion. The spectral absorption (0.2–5 μm) for snow grains internally mixed with BC/dust is confined to wavelengths shorter than about 1.4 μm, beyond which ice absorption predominates. Based on the single-scattering properties determined from stochastic and light absorption parameterizations and using the adding/doubling method for spectral radiative transfer, we find that internal mixing reduces snow albedo substantially more than external mixing and that the snow grain shape plays a critical role in snow albedo calculations through its forward scattering strength. Also, multiple inclusion of BC/dust significantly reduces snow albedo as compared to an equal-volume single sphere. For application to land/snow models, we propose a two-layer spectral snow parameterization involving contaminated fresh snow on top of old snow for investigating and understanding the climatic impact of multiple BC/dust internal mixing associated with snow grain metamorphism, particularly over mountain/snow topography.

1. Introduction

In our previous work, we developed a geometric-optics surface-wave approach for the computation of light absorption and scattering by complex and inhomogeneous particles for application to aggregates and snow grains with external and internal mixing structures [*Liou et al.*, 2011]. We demonstrated that a small BC particle on the order of 1 μm internally mixed with snow grains could effectively reduce visible snow albedo by as much as 5–10%. Subsequently, we applied this approach to contaminated ice particles in contrail cirrus and investigated the effects of internal and external mixing of BC in ice particles on the radiative forcings and heating rates of contrail cirrus [*Liou et al.*, 2013]. Also presented was a parameterization of the spectral extinction coefficient, single-scattering coalbedo, and asymmetry factor for contaminated ice particles for efficient application to radiative transfer calculations on the basis of the comprehensive spectral database for the single-scattering properties of pure ice particles of various shapes and sizes developed by *Yang et al.* [2013]. In conjunction with this study, we noted observations by *Petzold et al.* [1998, 1999] relative to plural numbers of BC particles inside and outside of contrail ice crystals.

Multiple internal mixing of BC/dust in snow grains can be produced by nucleation, accretion, riming, aggregation, and sintering during aerosol-cloud-precipitation processes known as wet deposition. Internal mixing can also occur via the direct or dry deposition of aerosols onto high elevation snow, followed by successive snow events. Mountain glaciers and polar ice sheets are excellent archives and imprints of atmospheric BC/dust particles associated with wet and dry depositions. *Ming et al.* [2008] conducted BC measurements in a 40 m ice core over the East Rongbuk Glacier in the northeast saddle of Mount Everest, which provided a historical record of BC deposition in the high Himalayas over the past 50 years. Additionally,

©2014. American Geophysical Union. All Rights Reserved.

Ming et al. [2009] collected BC concentrations from snow samples taken at a number of selected glaciers in west China during 2004–2006. Their findings revealed that BC concentrations are higher at lower elevation sites (Tienshan Mountains) than comparable samples obtained on the Tibetan Plateau, due likely to the topography effect. *Xu et al.* [2009] measured aerosol concentrations including BC in ice cores, spanning five Tibetan glaciers that illustrated an increasing deposition of anthropogenic aerosols during the period 1998–2005. *Hadley et al.* [2010] provided one of the first direct measurements documenting the efficient deposition of BC on Sierra Nevada snow packs while revealing high BC concentrations in falling snow. *Sterle et al.* [2013] showed that BC concentrations were enhanced sevenfold in surface snow compared to snowpack bulk values in the eastern Sierra Nevada from February to May 2009. Ice cores extracted from high elevations in the European Alps also displayed increasing BC concentrations from the era of the Industrial Revolution to the twentieth century [*Jenk et al.*, 2006; *Thevenon et al.*, 2009]. Based on a Single Particle Soot Photometer, *Schwarz et al.* [2013] illustrated that the modal volume-equivalent radius for BC particles in snow is about 0.1 μm. *Flanner et al.* [2012] pointed out that there could be up to 10^9 BC particles in a snow grain (>100 μm). With reference to dust, *Kumai* [1977] investigated the long-term variation of atmospheric aerosols in snow and deep ice core samples taken from Camp Century, Greenland, and showed that a majority of these aerosols were silicate mineral dust with a mean size on the order of 1 μm. *Hammer et al.* [1985] found dust in snow grains with a size on the order of 0.1 to 2 μm in Greenland ice cores. *Zdanowicz et al.* [1998] measured and compared the concentration, deposition rate, and size distribution of dust aerosols in snow pits on the Penny Ice Cap, Baffin Island, Arctic Canada with earlier studies. Also, *Zdanowicz et al.* [2006] measured the dustfall over snow packs in the St. Elias Mountains, Canada, indicating high dust concentrations found in snow in April 2001. *Kang et al.* [2010] used ice cores to reconstruct dust load history over the central Tibetan Plateau from 1940 to 2005 and found that dust loading in this region has increased since the 1990s peaking toward the end of the year.

From the instant snow hits the ground, it begins an endless process of metamorphism, which is a term in reference to the physical change of snow grains within a snowpack resulting from differences in temperature and pressure. Using a scanning electron microscopy technique in February 2002, *Dominé et al.* [2003] studied the natural metamorphism of snow samples collected near Chamrousse, a well-known ski resort town in the French Alps. The fresh snow was collected within minutes of its fall and immersed immediately in liquid nitrogen to preserve its shape and size. The sample pictures illustrate the wide variety of shapes and habits, including plates, columns, column rosettes, stellar and dendritic crystals, and various irregular crystals, all of which exhibit sharp angles. After 14 days of isothermal metamorphism, extensive changes occurred such that the original shapes were substantially modified with no sharp edges between two flat faces, leading to rounded crystals with different shapes. These snow grains are referred to as old snow. In view of these and other observations [e.g., *Aoki et al.*, 2000], we have used hexagonal plates/columns and Koch snowflakes, and spheroids, respectively, to model fresh and old snow grains for light scattering and absorption calculations.

This paper is organized as follows. In section 2, we present a stochastic approach to account for BC/dust multiple internal mixing in snow grains of various shapes, including hexagonal plate/column types (convex particles) and Koch snowflakes (concave particles), and develop a relationship between the BC/dust number concentration in snow grains and deposition rate. This is followed by a discussion in section 3 of light absorption and scattering by a snow grain internally mixed with multiple BC/dust particles and a group of such snow configurations using an improved geometric-optics approach developed in *Liou et al.* [2011, 2013] and *Takano et al.* [2013]. In section 4, we present computational results in terms of the single-scattering properties of a number of snow grain and BC/dust mixing states and shape factors, and the corresponding visible and spectral snow albedos. Herein, we propose a two-layer spectral snow model composed of fresh snow on the top and old snow on the bottom for parameterization purposes. Concluding remarks are given in section 5.

2. A Stochastic Approach to Parameterize BC/Dust Multiple Internal Mixing in Snow Grains

Internal mixing during wet and dry depositions cannot be entirely predicted by the first principal and must be governed by stochastic processes. To mimic the observed snow grain shape, we shall consider two types for fresh snow: Plate/column and Koch snowflakes. For old snow, we propose to use spheroids. The morphology of ice particles in the atmosphere is complex and intricate. However, to a good approximation and within the context of light scattering/absorption calculations, plates/columns and Koch snowflakes may

©2014. American Geophysical Union. All Rights Reserved.

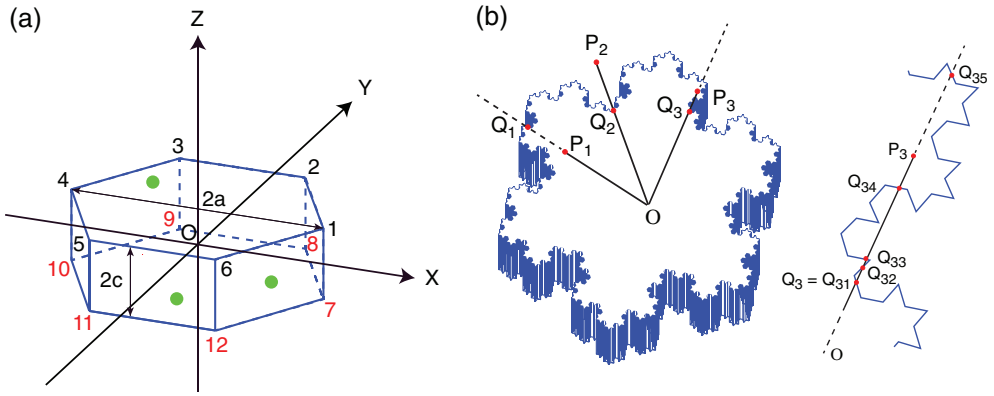

Figure 1. (a) Geometry for the internal inclusion of BC/dust particles inside a hexagonal plate (a convex-shaped particle) in the *xyz* coordinates where the numbers (1–12) denote the corner position of the hexagon defined by the diameter 2*a* in basal planes and the length 2*c* in the *c* axis. (b) A schematic diagram for a basal plane of a Koch snowflake of the order 4 in which the points P_i, (i = 1, 2, and 3) are determined by random numbers, and Q_i are points on the boundary of the snowflake, and Q_{ij} denotes subset points of Q_i to represent the concave condition of a Koch snowflake such that selected random points (BC/dust) are within it.

be used to represent defined shapes (such as bullet rosettes and column aggregates) and dendritic ice crystals, respectively. For aged snow, spheroids may be the best representation in terms of shape. For comparison purposes, we have also employed spheres, which are commonly assumed in light scattering and absorption calculations involving snow [e.g., *Wiscombe and Warren*, 1980; *Jacobson*, 2004; *Flanner and Zender*, 2006].

2.1. Hexagonal Plate/Column

Consider a 3-D plate shape containing two basal planes and six hexagonal side planes, as shown in Figure 1a. In order to insert and distribute a number of small particles inside this hexagonal plate, we may define a set of coordinate (x, y, z) stochastically as follows:

$$x = 2a'(\mathrm{RN} - 1/2), \tag{1}$$

$$y = 2\frac{\sqrt{3}}{2}a'(\mathrm{RN} - 1/2), \tag{2}$$

$$z = 2c'(\mathrm{RN} - 1/2), \tag{3}$$

where RN is a random number selected from a range [0, 1], and a' and c' are given by

$$a' = a - r_s, \tag{4}$$

$$c' = c - r_s, \tag{5}$$

where a and c (= $L/2$) are the radius and half height of a hexagon, respectively, and r_s is the radius of a sphere inside this hexagon defined in Figure 1a.

Next, we must check whether the point $P(x, y, z)$ is within the hexagonal crystal. Equations (2) and (3) ensure that the point is to the left of a plane "2-3-9-8" expressed by $y = (\sqrt{3}/2)a'$ and on the right of another plane "6-5-11-12" expressed by $y = -(\sqrt{3}/2)a'$, while it is below the plane defined by "1-2-3-4-5-6," which is expressed by $z = c'$, and above another plane defined by "7-8-9-10-11-12," which is expressed by $z = -c'$. In order for the randomly selected point to be inside the crystal, another four additional conditions must be satisfied:

$$y + \sqrt{3}x - \sqrt{3}a' < 0, \text{ for a particle to the left of the plane "1-2-8-7,"} \tag{6}$$

$$y - \sqrt{3}x + \sqrt{3}a' > 0, \text{ for a particle to the right of the plane "1-6-12-7,"} \tag{7}$$

$$y + \sqrt{3}x + \sqrt{3}a' > 0, \text{ for a particle to the right of the plane "5-4-10-11,"} \tag{8}$$

$$y - \sqrt{3}x - \sqrt{3}a' < 0, \text{ for a particle to the left of the plane "3-4-10-9."} \tag{9}$$

If equations (6)–(9) are not satisfied or the distance between internal spheres is less than $2r_s$, the point is discarded. The above process is repeated until the desired number of points N_s is reached. The stochastic

©2014. American Geophysical Union. All Rights Reserved.

generation of internal particles in an ice crystal can be applied to different habits, including bullet rosette, aggregate, hollow column, needle, as well as sphere and different types of spheroid.

2.2. Formation of a Koch Snowflake (Six-Side Symmetry)

We shall first consider an equilateral triangle and add three $\frac{1}{3}$ equilateral-sized triangles at the center of this triangle. Subsequently, on each side of the present six such triangles (12 sides), we carry out the same additions to yield 48 sides, and continue the process n times, which will lead to the formation of a Koch snowflake [*von Koch*, 1904]. Usually, $n = 4$ is sufficient for demonstration purposes. A Koch snowflake, which has the fractal dimension of 1.262, takes place only on side planes. However, the two basal planes are flat. Thus, a 3-D Koch snowflake contains two flat basal planes and 3×4^n highly irregular side planes (with six-side symmetry) associated with n fractal iterations (see Figure 1b, where $n = 4$). In order to conduct light scattering exercises, we must define the required surface area and volume. Let the length of an equilateral triangle be a. Then, its 2-D area is given by $A_o = \sqrt{3}/4a^2$. The area generated by n iterations is then given by

$$A_n = A_{n-1} + 3 \times 4^{n-1}/3^{2n} A_o. \tag{10}$$

The volume of a Koch Snowflake is simply $V_n = A_n L$, where L is the length defining the two basal planes. Also, the radius of a Koch snowflake can be defined by $a^* = \sqrt{3}/3a$. For comparison purposes, we may also define an equivalent sphere with a radius a_{eq} such that $V_n = 4\pi/3{a_{eq}}^3$.

The Koch snowflake depicted in Figure 1b is a concave shape which differs from the conventional convex ice particles. For this reason, we must modify the random generation program presented above to ensure all particles are inside the Koch snowflake. In addition to the preceding procedure, we may select $P_j(x_j, y_j)$ ($j = 1, 2, 3, \ldots$) to represent the points determined by random numbers due to the convex nature of the particle. Let the line intersection be denoted as $\overline{OP}_j$ and the boundary point of a Koch snowflake be denoted as Q_{3k} ($k = 1, 2, \ldots, 5$). As shown in the graph, P_1 is a point within the Koch snowflake. If $\overline{OP_2} > \overline{OQ_2}$, then P_2 is not a point within the Koch snowflake. In the case of P_3 and Q_3, we must consider whether P_3 is in the concave part of the Koch snowflake boundary (Figure 1b, left diagram). If $\overline{OP_3} < \overline{OQ_{31}}$, $\overline{OQ_{32}} < \overline{OP_3} < \overline{OQ_{33}}$, or $\overline{OQ_{34}} < \overline{OP_3} < \overline{OQ_{35}}$, then P_3 is a point within the Koch snowflake. Otherwise, P_3 is not a point within the Koch snowflake. Once the points $P_j(x_j, y_j)$ are in the x-y plane, then the same procedure for the plate case described in equation (3) can be followed.

2.3. Relating BC/Dust Number Concentration in Snow Grains to Deposition Rate

In the preceding subsections, we have developed a stochastic approach to place multiple particles inside a plate/column type of snow (convex) and a Koch snowflake (concave). We must now relate the total number of BC/dust particles inside a snow grain to their concentration in units of parts per million by mass (ppm), which are related to deposition rate, a model parameter.

Consider an equal-volume spherical snow grain (with reference to a plate/column or a Koch snowflake) whose radius is defined by r_{snow} (μm), and let N_s be the total number of BC/dust particles whose radius is r_{aero} (μm). The BC/dust total concentration C is defined by

$$C = D_{aero}/D_{snow} = M_{aero}/M_{snow} = N_s \rho_{aero} {r^3}_{aero}/\rho_{snow} {r^3}_{snow}, \tag{11}$$

where D (mass/area/time) and M denote the deposition rate and mass, respectively, and ρ_{aero} and ρ_{snow} are BC/dust and snow densities (g/cm^3), respectively. If ρ_{aero}, ρ_{snow}, r_{aero}, and r_{snow} are known, then the total BC/dust concentration (ppm) and total number of BC/dust particles are related by the following: $C = k_1 N_s$, where k_1 is a certain constant. Using BC as an example, if $r_{aero} = 0.1$ μm and $r_{snow} = 100$ μm, then the BC concentration C of 1 ppm corresponds to the BC number N_s of 458 inside a snow grain. The single-scattering properties of a snow grain containing N_s absorbing BC/dust particles can then be determined from the light scattering and absorption program described in section 3.

2.4. Relating Snow Water Equivalent to Snow Optical Depth

In order to compute the albedo of a snow layer comprising a group of snow grains with internally (or externally) mixed BC/dust particles, the optical depth of the layer is required. In their pioneering paper, *Wiscombe and Warren* [1980] derived the snow optical depth in terms of the equivalent depth of liquid water in snowpack assuming spherical snow grains. In land-atmosphere interaction studies, snow water equivalent

©2014. American Geophysical Union. All Rights Reserved.

(SWE) is a common snowpack measurement, which is an important parameter defined as the depth of water (d) that would theoretically result if the entire snowpack is melted instantaneously. SWE is generally expressed in terms of daily value and its relation to d is as follows:

$$\text{SWE}\ \left(\text{in units of kg/m}^2\right) = \rho_{\text{ice}} \times d, \tag{12}$$

where ρ_{ice} is the snow density (~0.45 g/cm^3).

Consider now a group of hexagonal snow grains. The average geometric cross section is given by

$$G = 3a^2\left[\sqrt{3} + 4(L/2a)\right]/4, \tag{13}$$

and the volume of snow grains, which is $1/N$, where N is the total number of snow grains, can then be expressed by

$$V = 3\sqrt{3}a^3(L/2a), \tag{14}$$

where L is the crystal length and a is the radius of a hexagon.

The optical depth of a snow layer is defined by

$$\tau_s = N\sigma_{\text{ext}}d, \tag{15}$$

where σ_{ext} is the extinction coefficient of a snow grain. Thus, the optical depth can be expressed in the form

$$\tau_s = \text{SWE}\, G\, Q_{\text{ext}}/V\rho_{\text{ice}}, \tag{16}$$

where Q_{ext} is the extinction efficiency (= σ_{ext}/G), which is approximately equal to 2 for snow grains. It follows that the optical depth of a snow layer can be directly related to SWE once the size (G and V) of a snow grain is given. If we assume SWE = 4.2 kg/m^2, a reasonable value for new snow (corresponds to ~0.93 cm new snow depth), a = 126.3 μm and $L/2a$ = 0.4, we obtain a value of τ_s of about 200. Note that *Aoki et al.* [2011] assumed that $0 <$ SWE $<$ 10 kg/m^2 in their snow albedo analysis.

3. Light Absorption and Scattering by a Snow Grain Internally Mixed With Multiple BC/Dust Particles

It appears that the exact analytic and/or numerical solutions to determine the single-scattering properties of a snow grain containing N_s internally mixed BC/dust particles cannot be derived on the basis of the conventional wave equations and boundary conditions due to the complex and intricate nature of 3-D geometric configuration. However, we may follow the improved geometric-optics approach developed by *Liou et al.* [2011, 2013] and *Takano et al.* [2013] for application to BC aggregates, and *Liou et al.* [2013] for application to irregular ice crystal contaminated by one BC/dust. In particular, *Takano et al.* [2013] followed the geometric-optics surface-wave (GOS) approach coupled with the Rayleigh-Gans-Debye (RGD) adjustment for application to size parameters smaller than approximately 2, the results of which are compared with those determined from the superposition T matrix method. It is shown that under the condition of random orientation, the single-scattering results computed from GOS/RGD are in general agreement with those from the T matrix approach and with limited measured absorption data.

3.1. Single Snow Grains

In geometric optics, the geometric reflection and refraction can be carried out by using hit-and-miss Monte Carlo photon tracing once the snow grain shape and the number of internally mixed BC/dust positions are defined by the stochastic processes described in subsection 2.1 for convex crystals such as plate/column and other conventional ice crystal shapes and subsection 2.2 for concave Koch snowflakes. Following the improved geometric optics approach developed in *Yang and Liou* [1997] and *Liou et al.* [2010], the extinction (σ_e) and absorption (σ_a) cross sections for a single snow grain containing N_s internally mixed BC/dust particles can be written as follows:

$$\sigma_e = \frac{2\pi}{k^2}\text{Re}\left[S_{11}(\hat{e}_0) + S_{22}(\hat{e}_0)\right], \tag{17}$$

$$\sigma_a = \sum_{\gamma}\sum_{p=1}^{\infty}\left(t_1^2 r_1^{p-1} + t_2^2 r_2^{p-1}\right)/2\exp\left(-2k\sum_{j=1}^{p-1} m_{i,j}d_j\right)\left[1 - \exp\left(-2\text{km}_{i,p}d_p\right)\right], \tag{18}$$

where k is the wave number, Re denotes the real part, S_{11} and S_{22} are two diagonal elements of the scattering

©2014. American Geophysical Union. All Rights Reserved.

amplitude matrix in the forward direction, and $\hat{e}_0$ denotes the incident direction. The term $t_j^2 r_j^{p-1}$ ($j = 1, 2$) in equation (18) represents the cumulative product of Fresnel coefficients, the subscript index p (= 1, 2, 3, …) denotes the internal localized ray, γ in the first summation of the absorption cross section is associated with all incident photons impinging onto BC/dust particles assuming spherical shape, $m_{i,j(\text{or } p)}$ represents the imaginary refractive index for an inhomogeneous sphere, and $\boldsymbol{d}_{j(\text{or } p)}$ denotes a vector distance between two points.

3.2. A Group of Snow Grains

Consider a group of snow grains randomly oriented in space and define an effective geometric cross-section area to evaluate the extinction and absorption efficiencies. Let A be the area of a square sufficiently large to cover the geometric cross section of a snow grain and set this square to be L^2, where L denotes the particle's maximum dimension. Further, let N_a be the number of photons incident on this snow grain, which is dependent on the particle's orientation, and N_t be the number of total photons used in the calculation. The effective geometric shadow of a snow grain on a plane perpendicular to the incident light beam propagating along the z axis direction can therefore be defined as follows:

$$A_s(\alpha, \beta) = A \times [N_a(\alpha, \beta)/N_t], \tag{19}$$

where α and β are angles which denote the orientation of a snow grain in a two-dimensional plane with reference to the incident light beam. It follows that for an ensemble of randomly oriented snow grains, the extinction and absorption efficiencies averaged over all orientations can be written in the form

$$Q_{\text{ext,abs}} = \int_\alpha \int_\beta \sigma_{e,a}(\alpha, \beta)\ \cos\alpha \, \mathrm{d}\alpha \mathrm{d}\beta / \int_\alpha \int_\beta A_s(\alpha, \beta) \cos\alpha \, \mathrm{d}\alpha \mathrm{d}\beta. \tag{20}$$

The improved geometric-optics approach also includes diffraction component. The original theoretical development of diffraction begins with Babinet's principle, which states that the diffraction pattern in the far field (Fraunhofer diffraction) from a circular aperture is identical to that from an opaque disk or sphere of the same radius. To apply this principle to randomly oriented nonspherical particles, we may use the effective geometric cross-section area defined in equation (19). Thus, the diffracted intensity I_d for an ensemble of randomly oriented snow grains can be expressed by [*Born and Wolf*, 1975; *Liou*, 2002; *Liou et al.,* 2011]

$$I_d \propto \int_\alpha \int_\beta \left| \int_{A_s} \exp[-ikr(x, y, \alpha, \beta)] \mathrm{d}x \mathrm{d}y \right|^2 \cos\alpha \, \mathrm{d}\alpha \mathrm{d}\beta, \tag{21}$$

where r is the distance between a point in the shadow A_s and a distant point from the shadow. Analytical solutions for equation (21) exist only for simple nonspherical shapes, such as column, plate, and spheroid [*Takano and Liou*, 1989, 1995; *Takano et al*., 2012]. From the total scattered intensity, we define a parameter referred to as the asymmetry factor as follows:

$$g = \frac{1}{2} \int_{-1}^{1} P_{11}(\cos\Theta) \cos\Theta \, \mathrm{d}\cos\Theta, \tag{22}$$

where $P_{11}(\Theta)$ denotes the normalized phase function, which is directly related to the total scattered intensity, as a function of the scattering angle Θ. The g factor is the first moment of the phase function and represents the strength of forward scattering.

In the preceding analysis, we have postulated that the conventional independent scattering concept for a sample of randomly oriented snow grains can be applied, such that each snow grain intercepts the incident waves and undergoes the scattering and absorption processes in exactly the same way as if all other snow grains did not exist. This can be applied to aerosol and cloud particles, which are sufficiently separated in the atmosphere to satisfy the required condition. The concept of independent scattering allows for the use of energy quantity instead of electric field in the analysis of the propagation of electromagnetic waves. *Wiscombe and Warren* [1980] discussed in detail the effects of interparticle interference due to close packing of snow grains on the single-scattering calculations and argued that this interference effect appears to be negligible for snow albedo calculations using observed data as a reference. Of course, a more fundamental understanding of the effect of close packing of snow grains on light absorption and scattering could be a subject for further research.

©2014. American Geophysical Union. All Rights Reserved.

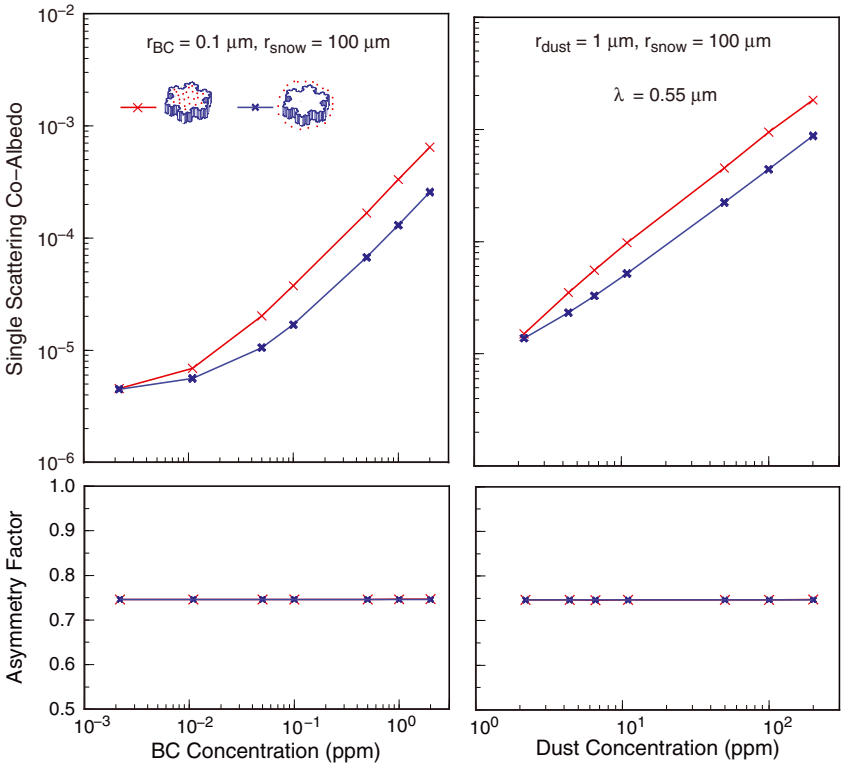

Figure 2. Single-scattering coalbedo and asymmetry factor for Koch snowflakes (100 μm volume-equivalent radius) internally and externally mixed with BC (0.1 μm radius) and dust (1 μm radius) as a function of their concentrations at a wavelength of 0.55 μm. The BC/dust concentration is related to the total BC/dust number inside and outside of the snowflake.

4. Computational Results and Discussion

4.1. Single-Scattering Properties

4.1.1. Internal Versus External Mixing

We first investigate the single-scattering coalbedo ($1 - \varpi$) (= absorption cross section/extinction cross section) and the asymmetry factor g for randomly-oriented Koch snowflakes internally and externally mixed with BC/dust using the 0.55 μm wavelength. The Koch snowflake has the same volume as a sphere with a radius r_{snow} of 100 μm and an aspect ratio $L/2a^*$ of 0.4, where L is the length along the c axis and $2a^*$ is the diameter of a Koch island. BC/dust aerosols are assumed to be spheres with a radius r_{BC} of 0.1 μm and r_{dust} of 1 μm. ($1 - \varpi$) for the case of internal mixture is larger than that for external mixture, as shown in Figure 2. For BC concentration ranging from 2×10^{-3} to 2 ppm [*Ming et al.*, 2009], the internal mixing case shows stronger absorption than its external counterpart as a function of BC ppm. The ($1 - \varpi$) ratio between the two is on the order of 2.5 for BC concentrations of 10^{-1} to 2 ppm. For a very small BC concentration of 2×10^{-3} (one BC particle of 0.1 μm), the effect on snow absorption is about the same for the two mixing cases and is extremely small. The general increase in absorption in the case of internal mixing is due to enhancement of multiple photon absorption inside the snow grain. The dust deposition is generally larger than BC and we have set the range from 2 to 2×10^2 ppm [*Zdanowicz et al.*, 2006]. Since the absorption power of dust ($1.53 - i0.008$ refractive index) is less than that of BC ($1.833 - i0.74$ refractive index), the ($1 - \varpi$) ratio is smaller, with a value on the order of 2 for dust concentration from 10 to 10^2 ppm. A final note is in order: The asymmetry factor is primarily governed by the snow grain size regardless of BC/dust mixing states. We see an asymmetry factor of ~0.75 for a Koch snowflake with an equivalent spherical radius of 100 μm.

In terms of internal and external mixing issue, we note the following work. *Grenfell et al.* [1994] discussed the effect of external and internal mixtures of BC in snow grains. *Doherty et al.* [2010] reported a study of the content of light-absorbing impurity, specifically BC, in Arctic snow. *Grenfell et al.* [2011] presented measurements of spectral absorption for snow contaminated by BC.

©2014. American Geophysical Union. All Rights Reserved.

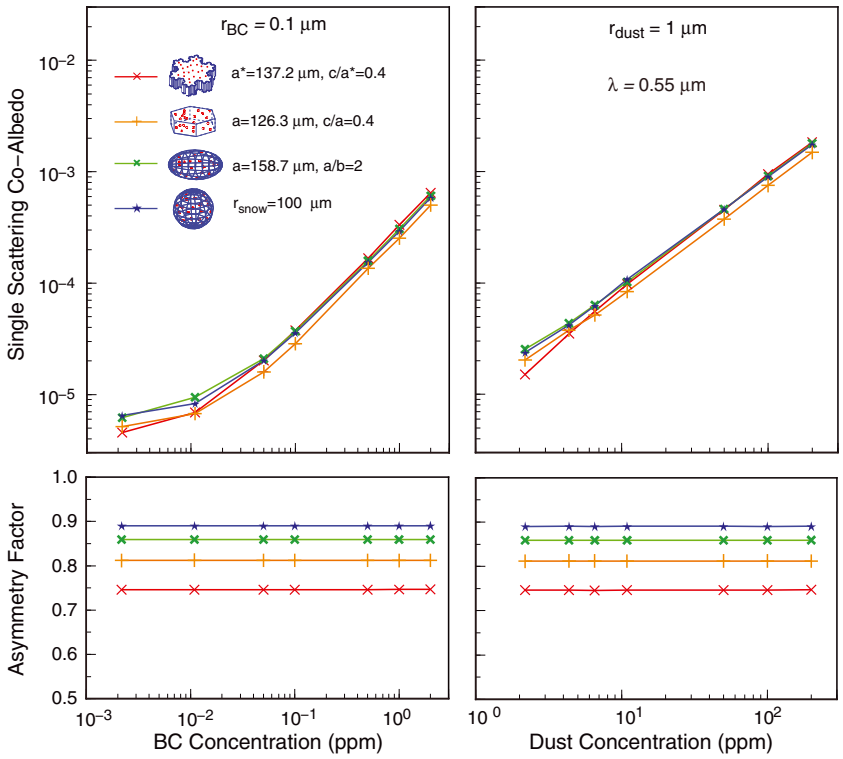

Figure 3. Comparison of the single-scattering coalbedo and asymmetry factor for volume-equivalent Koch snowflakes, hexagonal plates, and prolate spheroids as well as spheres contaminated by internally mixed BC (0.1 μm) and dust (1 μm) particles generated by a stochastic process at 0.55 μm. The volume-equivalent radius a (or a^*) and the associated aspect ratio for nonspherical snow grains are defined in the graphs.

4.1.2. Snow Grain Shape Effect

We study the effect of snow grain shape on the single-scattering albedo and asymmetry factor using the following four 3-D shapes: Koch snowflake, hexagonal plate, prolate spheroid, and sphere with an equivalent radius of 100 μm (Figure 3). In this manner, the four particle shapes have the same volume. Minor differences in $(1-\varpi)$ values among these four shapes are associated with their average geometric cross-sectional areas, which can affect photon interception as well as the internal distribution of BC/dust within different shapes. With respect to the asymmetry factor, smooth spheres have the largest value of 0.89 in view of strong scattering in the forward direction, whereas the Koch snowflakes have a minimal value of 0.746 because of highly irregular surfaces reducing forward scattering. The scattering processes produced by hexagonal plates and prolate spheroids fall between the preceding two shapes with values of 0.812 and 0.859, respectively. As noted previously, the asymmetry factor for snow grains is independent of multiple inclusions of BC/dust. Accordingly, the shape effect on absorption is small if the distribution of multiple inclusions remains the same; however, it has a substantial impact on the asymmetry factor, which will in turn affect radiative transfer calculations. Note that the snowflake asymmetry factor value of 0.746 is comparable to the asymmetry factor of ice crystals (0.74–0.75) measured by *Gerber et al.* [2000] and *Garrett et al.* [2003].

4.1.3. Multiple Versus Single Internal Mixing

If all internally mixed BC particles collide together as a single sphere with the same volume, what would be the difference in absorption between the two configurations? Assuming that this large sphere is located at the center and using 0.01, 0.1, and 1 ppm in the calculations, we find that substantial reductions in $(1-\varpi)$ occur, as shown in Figure 4. The largest difference is seen for a Koch snowflake, with a value of more than a factor of 10 (from $\sim 10^{-4}$ to $\sim 10^{-5}$), while the spherical snow grain displays the smallest difference. The multiple small BC particles within a large snow grain have a greater probability of trapping the photons impinging them as compared to a single large BC located at the center, on the basis of the improved geometric photon tracing approach we developed for the computation [see also *Jacobson*, 2006, 2012]. If the large BC particle is placed at other locations inside the snow grain, the results are similar. Several studies have

©2014. American Geophysical Union. All Rights Reserved.

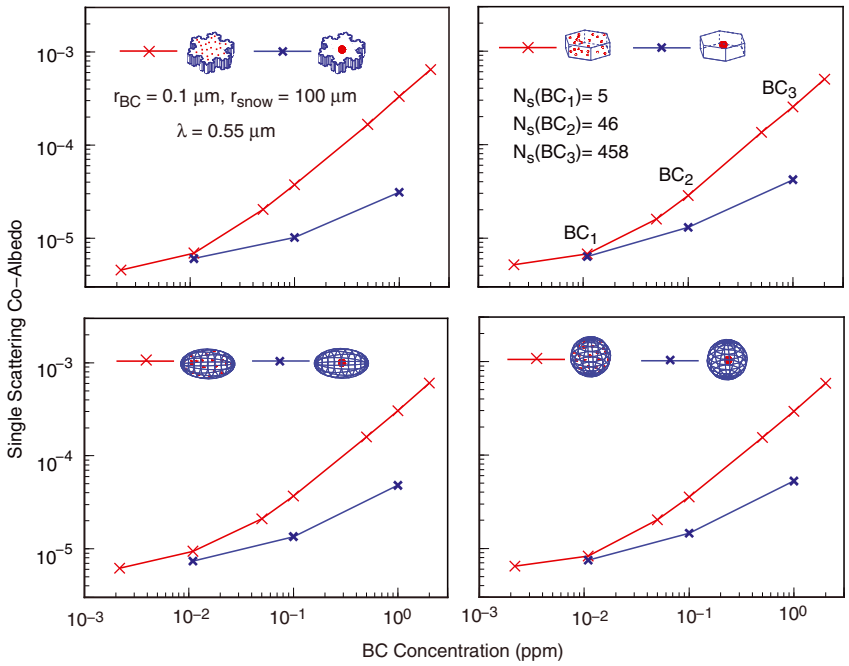

Figure 4. The single-scattering coalbedo for the three nonspherical snow grains with volume-equivalent spherical radii of 100 μm and spheres (100 μm radii) for two internal mixing configurations as a function of BC concentration at 0.55 μm. One represents randomly located BC particles (0.1 μm radius) in snow grains generated by a stochastic process, while the other denotes a single BC sphere having the same volume located at the center of snow grains. The term N_s (BC_i, i = 1, 2, and 3), applicable to all panels, denotes three total BC number in snow grains corresponding to BC concentrations of 0.01, 0.1, and 1 ppm.

presented light scattering solutions for an arbitrarily located inclusion in a sphere [*Borghese et al.*, 1992; *Fuller*, 1995; *Videen and Chýlek*, 1998]. *Chýlek et al.* [1984] considered randomly distributed soot particles in a water drop of 5 μm and developed a mixing rule to obtain a mean refractive index, followed by Lorenz-Mie calculations for the contaminated sphere. Also, *Macke et al.* [1996] developed a light scattering program involving a spherical soot particle in a hexagonal ice crystal.

Finally, it should be pointed out that the refractive index of water is 1.33 in the visible, which is very close to that of ice (1.31). Thus, spherical results presented in Figure 4 are applicable to raindrop sized particles as well.

4.1.4. Single Internal Mixing—Aggregate Versus Sphere

Figure 5 shows $(1 - \varpi)$ for a Koch snowflake internally mixed with a diffusion-limited aggregate [see *Friedlander*, 2000; *Liou et al.*, 2011] consisting of 256 spherules and an equal-volume spherical BC particle at the center as a function of its radius r_{BC} and the ratio of $(1 - \varpi)$ (right, y axis). Figure 5 (left) shows that $(1 - \varpi)$ for a Koch snowflake with a radius r_{snow} of 100 μm increases monotonically with BC radius. The Koch snowflake containing aggregated BCs absorbs more light than its counterpart comprising the equal-volume spherical BC. For r_{BC} = 0.5 and 1 μm, the $(1 - \varpi)$ ratios are 3.914 and 4.838, respectively, slightly larger than the ratio of the average geometric cross-sectional area of an aggregate with reference to the equal-volume sphere of 3.875 associated with more internally reflected photons incident onto the former than the latter as size increases. For the smallest BC radius of 0.1 μm used in the calculation, ice absorption is stronger than BC absorption, producing a value of about 1 for the ratio of $(1 - \varpi)$. Figure 5 (right) shows $(1 - \varpi)$ results for a Koch snowflake of 1000 μm radius. Owing to its large size, ice absorption predominates resulting in an almost constant $(1 - \varpi)$.

4.1.5. Entire Solar Spectrum

In single-scattering calculations covering the entire solar spectrum (0.2–5 μm), we have employed the following sources for refractive indices: ice [*Warren and Brandt*, 2008], BC [*Krekov*, 1993; *d'Almeida et al.*, 1991], and dust [*d'Almeida et al.*, 1991]. For illustration purposes, we have used a hexagonal plate with an aspect ratio of $L/2a$ = 0.4 and an equivalent spherical radius of 100 μm for fresh snow grains [*Dominé et al.*, 2003], along with a BC radius of 0.1 μm and a dust radius of 1 μm. A prolate spheroid with an aspect ratio of a/b = 2

©2014. American Geophysical Union. All Rights Reserved.

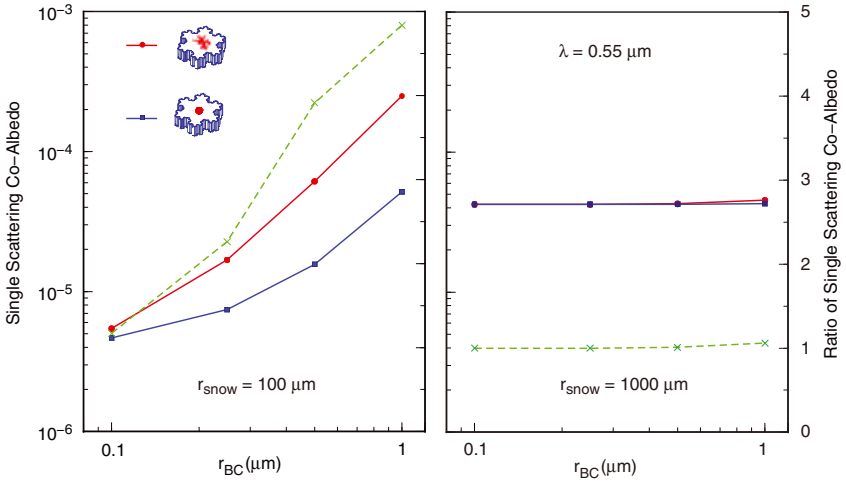

Figure 5. The single-scattering coalbedo for Koch snowflakes with spherical volume-equivalent radii of 100 and 1000 μm comprising an internally mixed BC aggregate consisting of 256 spherules generated by diffusion-limited processes [*Friedlander*, 2000] (red curve) and a volume-equivalent BC sphere (blue curve) located at the center for 0.55 μm wavelength. Also shown are ratios of the single-scattering coalbedo for the two snowflake sizes (green curve) using a different ordinate (*y* axis on the right).

and an equivalent spherical radius of 1000 μm is used for old snow [*Aoki et al.*, 2000]. Figure 6 displays the spectral $(1-\varpi)$ and *g* factor for fresh and old snow for a range of BC/dust concentrations. $(1-\varpi)$ for hexagonal plates internally mixed with BC/dust increases with increasing BC/dust concentration for wavelengths shorter than 1.4 μm, beyond which ice absorption takes over. At visible wavelengths, $(1-\varpi)$ is close to a constant value for BC (Figure 6, top left), but it shows a minimum for dust (Figure 6, top middle) in association with differences in the imaginary refractive indices. The $(1-\varpi)$ pattern for pure snow mimics variability of the ice imaginary refractive index and generally increases with increasing wavelength. Several remarkable maximum values located at 1.49, 2.0, and 2.85 μm (Figure 6, left and middle columns) are noted for the *g* factor independent of BC/dust contamination. These features are produced by strong ice absorption. The maximum, shown at 2.85 μm, is referred to as the Christiansen effect [*Christiansen,* 1884, 1885], which occurs when the real part of the refractive index approaches 1, while the corresponding imaginary counterpart is substantially larger, resulting in the domination of absorption, leading to sharp diffraction peaks in phase functions. Figure 6 (right column) shows relatively featureless $(1-\varpi)$ and *g* factor patterns for prolate spheroidal snow due to its large size and therefore large absorption. The extinction efficiencies for the above-mentioned snow grains in the solar spectrum are depicted in Figure 6, bottom row. Fluctuations in extinction efficiencies occur in the wavelength region from 0.2 to 2.6 μm for hexagonal plates with a radius of 100 μm due to the nature of interferences between diffraction and reflection/refraction, as well as insufficient computational points to resolve substantial variations in the complex refractive indices for ice, BC, and dust. A large fluctuation is seen at the 2.85 μm Christiansen region. For prolate spheroidal snow grains with an equivalent spherical radius of 1000 μm, fluctuations vanish as a result of extremely large size parameters.

4.2. Snow Albedo

4.2.1. Single Wavelength (0.55 μm)

Figure 7 shows the snow albedo of a semiinfinite snow layer for a solar zenith angle θ_0 of 60° as a function of BC/dust concentrations computed by the adding/doubling method for radiative transfer. Figure 7 (top) is for Koch snowflakes and spheres internally and externally mixed with BC/dust particles corresponding to the single-scattering parameters presented in Figures 2 and 3. Snow albedo decreases with increasing BC/dust concentrations such that the internal mixing case reduces more than its external mixing counterpart. For example, the difference between the two is about 5% for a BC concentration of 1 ppm. This reduction is primarily caused by absorption differences between the two mixing states. Figure 7 (bottom) depicts the snow grain shape effect using the data displayed in Figure 3, where the *g* factor, which is independent of the mixing states, plays a critical role in snow albedo calculations. We have

©2014. American Geophysical Union. All Rights Reserved.

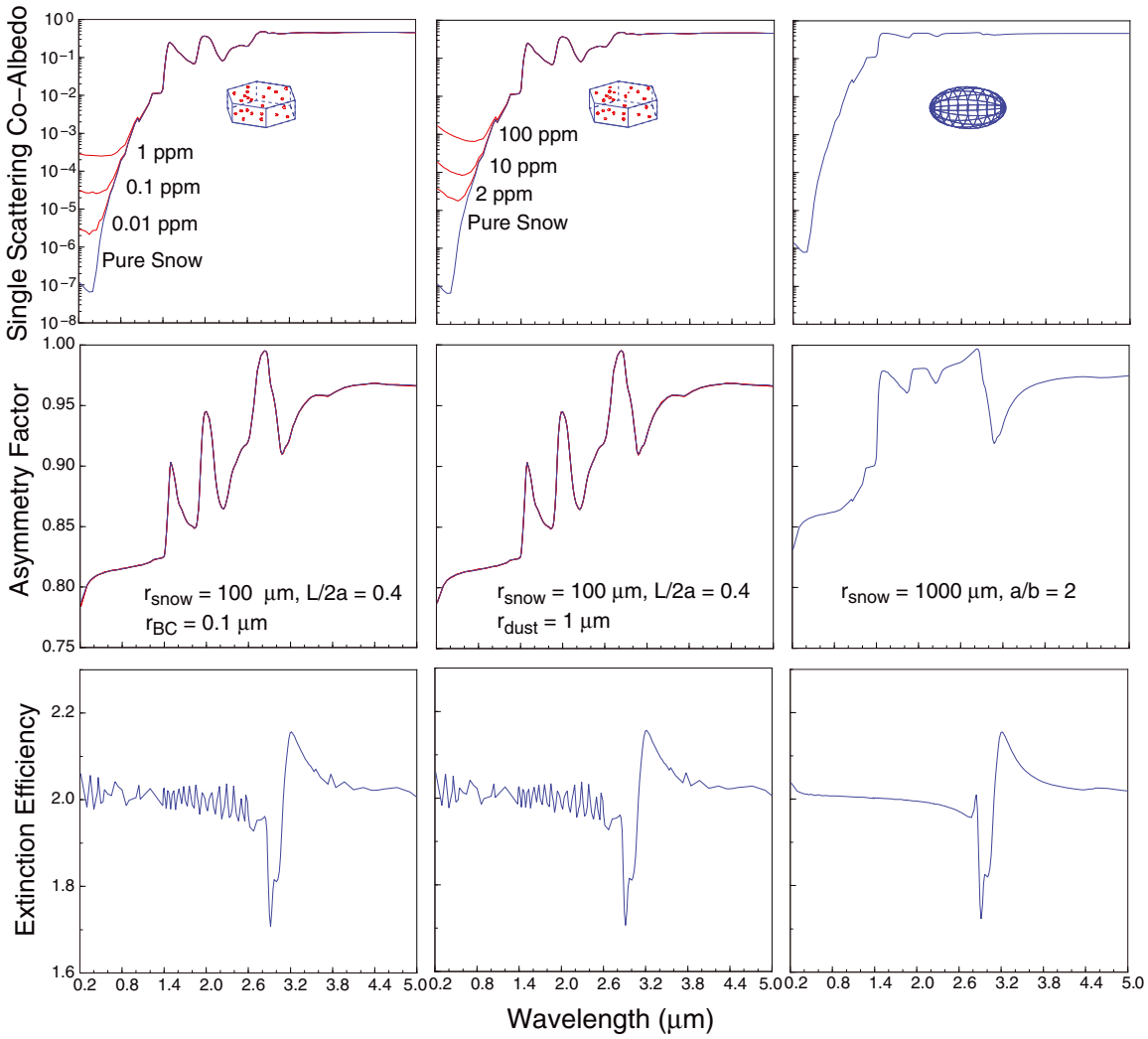

Figure 6. The single-scattering coalbedo, asymmetry factor, and extinction efficiency for hexagonal plate snow grains (representing new snow) contaminated with internally mixed (left column) BC and (middle column) dusts and for (right column) spheroid (representing old snow without contamination) as a function of wavelength. Hexagonal plate snow grains have an aspect ratio of 0.4 and a volume-equivalent spherical radius of 100 μm. Prolate spheroid snow grains have an aspect ratio of 2 and the volume-equivalent spherical radius of 1000 μm.

illustrated that due to their relatively weak forward scattering, Koch snowflakes reflect more light beams than the spherical shape. Snow albedos corresponding to spheroid and plate shapes are in between those of sphere and snowflake shapes.

Figure 8 illustrates snow albedo as a function of BC concentration for the four shapes: Koch snowflake, hexagonal plate, prolate spheroid, and sphere. The radius of these snow grains $r_{snow} = 100$ μm, but with two different configurations in the state of internal mixing. One contains a distribution of multiple BC particles with a radius of 0.1 μm generated by a stochastic process, while the other consists of a single particle located at the snow grain center, which has the same volume. Snow albedo differences are caused by the $(1 - \varpi)$ or absorption effect and are explained in the following. Let the geometric cross section for N_s multiple BCs with radius r_m be A_m and for a single BC with radius r_s be A_s. Because the volume for the two are the same, we have $N_s(4\pi/3)r_m^3 = (4\pi/3)r_s^3$. Thus, $r_s = N_s^{1/3} r_m$. The ratio of the two geometric cross sections is then given by $R_A = A_m/A_s = N_s \pi r_m^2/\pi r_s^2 = N_s^{1/3}$. If the BC concentration is 1 ppm, N_s is 458, leading to R_A of 7.71. This implies that the geometric cross section for absorption in the multiple inclusion case is 7.71 times larger than that in the single inclusion. In connection with this, the ratio of $(1 - \varpi)$ for multiple inclusion to single inclusion ranges from 5.6 to 10.7, with the largest value corresponding to Koch snowflakes, which can also trap additional

©2014. American Geophysical Union. All Rights Reserved.

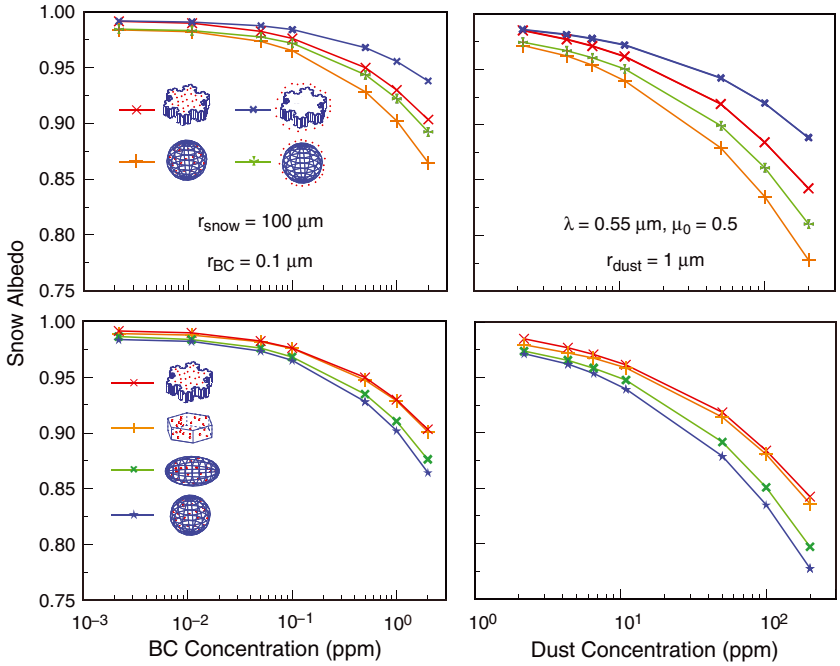

Figure 7. (top) The snow albedos for Koch snowflakes and spheres mixed with BC/dust particles internally and externally as a function of concentration at 0.55 μm. (bottom) The snow albedos for Koch snowflake, hexagonal plate, prolate spheroid, and sphere with a radius of 100 μm with internally mixed BC/dust particles as a function of concentration. The four snow grain shapes have the same volume. Both the single-scattering coalbedo and the asymmetry factor are required (see Figure 3) in radiative transfer calculations.

photons. Moreover, the snow albedo reduction in the case of multiple inclusions is also governed by snow grain shape associated with the *g* factor.

4.2.2. Comparison With Previous Studies for External Mixing Cases

In a comprehensive study, *Aoki et al.* [2011] developed a spectral snow albedo model, which accounts for snow grain size and externally mixed BC/dust concentration as a function of layer structure and Sun position. Figure 9 (top) depicts a comparison of solar albedo for visible (VIS), near-infrared (NIR) and shortwave (SW) bands presented in Figure 7b of the paper by *Aoki et al.* [2011]. In our adding-doubling radiative transfer calculations, we used the same input, including the top and bottom layers consisting of a snow grain radius of 50 μm externally mixed with BC and of 1000 μm, respectively. The present results corresponding to three BC concentrations of 0.01, 0.1, and 1 ppm are overlaid using red triangles and show excellent comparison. Figure 9 (bottom) compares the spectral snow albedo from 0.3 to 1.5 μm of a semiinfinite optical depth layer presented in *Warren and Wiscombe* [1980, Figure 7a] who used the delta-Eddington approximation in radiative transfer calculations. The spherical snow grain radius is 100 μm externally mixed with BC particles with a radius of 0.1 μm. Again, excellent agreement between the two model calculations is illustrated, except for minor differences seen in wavelengths larger than 1 μm, which are mostly likely due to different complex refractive indices [*Irvine and Pollack*, 1968] used in their early pioneering work.

The optical depths for snow layers employed in these two studies are semiinfinite; thus, snow absorption is approximately equal to one minus snow albedo. In terms of measurements, *Aoki et al.* [2011] conducted snow albedo measurements at Sapporo, Hokkaido, Japan, during two winters from 2007 to 2009. Theoretical results computed from Aoki et al.'s program and the present approach using external mixing show good agreement with measured data.

4.2.3. Two-Layer Snow Model

We have built a two-layer spectral snow model composed of fresh snow on the top and old snow on the bottom. Figure 10 shows the spectral albedo of a two-layer snow grains as a function of wavelength for the solar zenith angle θ_0 of 60° using the single-scattering properties depicted in Figure 6. The top new snow layer is composed of hexagonal plates with a radius of 100 μm internally mixed with BC (Figure 10, top) and dust (Figure 10, bottom). The optical depth of the snow layer is primarily determined by pure snow with a

©2014. American Geophysical Union. All Rights Reserved.

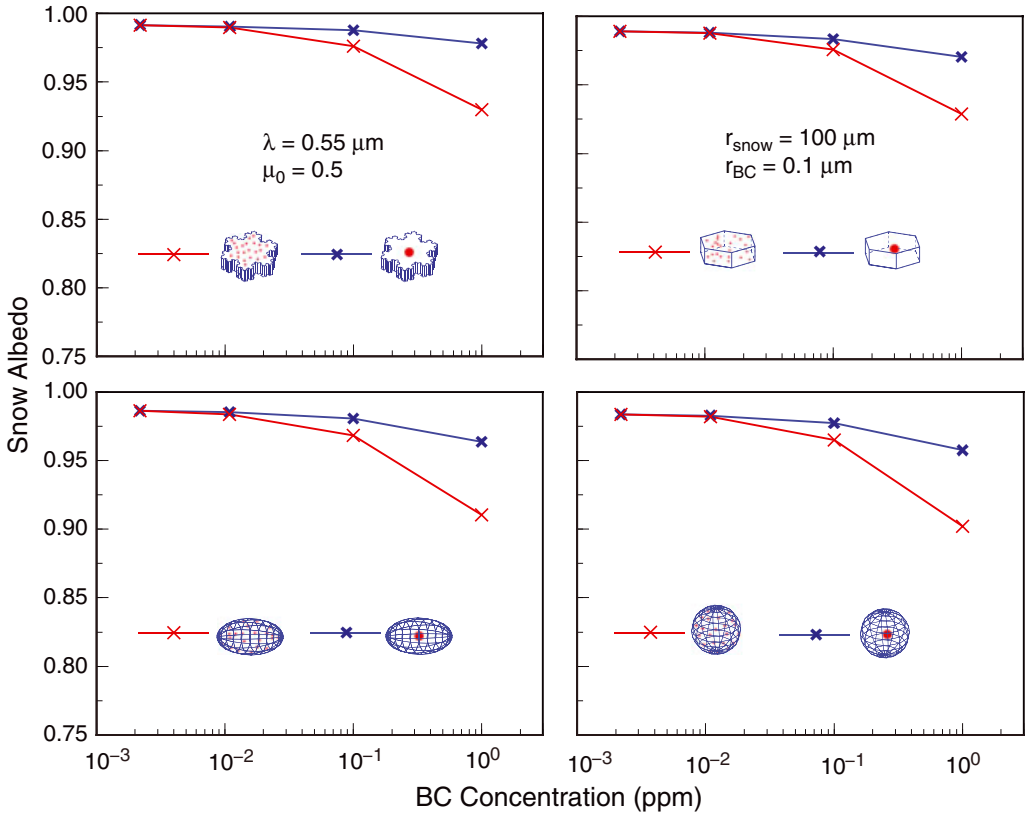

Figure 8. Snow albedo for the four snow grain shapes with a radius of 100 μm in two internal mixing configurations at 0.55 μm as a function of BC concentration. One configuration represents random location of internally mixed BC particles with a radius of 0.1 μm generated by a stochastic process, while the other denotes a single BC particle with the same volume located at the center of a snow grain.

value of about 200 in the visible. The bottom snow layer, containing old snow assumed to be spheroids with a radius of 1000 μm, is considered to be semiinfinite. Corresponding to Figure 6 (left and middle columns), the effect of internally mixed BC/dust on snow albedo occurs at wavelengths < 1.4 μm, and the degree of reduction is governed by BC/dust concentration. The 1.4 μm snow albedo reduction limit was also shown in *Warren and Wiscombe* [1980] and *Jacobson* [2004, 2006]. The inserted diagrams illustrate enlarged albedo scales as a function of wavelength from 0.2 to 1 μm to highlight snow albedo reduction. For a 1 ppm BC concentration, we see a reduction of about 7% in the UV and VIS, while in the NIR, it is much less. For a 100 ppm dust concentration, the reduction in snow albedo has a maximum value of about 12% in the VIS. Given the same size, the absorption of dust is less than that of BC associated with smaller values in the imaginary part of the refractive index. However, dust normally has a larger size (~1 μm) than BC (~0.1 μm).

5. Concluding Remarks

We have developed a stochastic approach to model the multiple inclusions of BC/dust particles for two types of snow grains: Plate/column types (convex) and Koch snowflakes (concave). Once the internally mixed BC/dust particles are in position, we can then conduct light absorption and scattering for contaminated snow grains by means of an improved geometric-optics approach coupled with the Monte Carlo photon tracing technique to compute their single-scattering properties. We carried out single-scattering calculations (extinction efficiencies, single-scattering coalbedo, and asymmetry factor) involving a group of snow grains using random orientation, a reasonable assumption since the possibility of preferred orientation of complex snow particles would appear to be small. The potential interference effect due to close packing in the case of wet and old snow was considered to be negligible following the argument presented in *Wiscombe and Warren* [1980].

©2014. American Geophysical Union. All Rights Reserved.

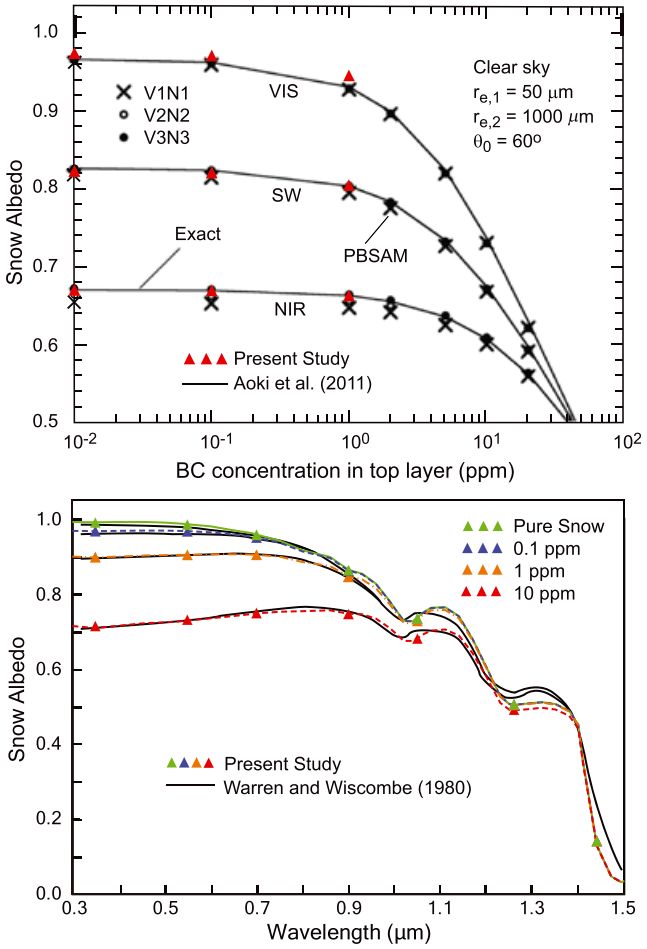

Figure 9. (top) The comparison of snow albedo as a function of BC concentration with results presented by *Aoki et al.* [2011, Figure 7b]. Color bold triangles represent the present computational values using the same input, which are overlaid onto their black-white curves. (bottom) The comparison of the snow albedo for a semiinfinite optical depth computed from the delta-Eddington method for radiative transfer with the results presented by *Warren and Wiscombe* [1980, Figure 7a]. In these calculations, the snow model involves spherical BCs (0.1 μm) externally mixed with spherical snow grains (100 μm).

We investigated a number of issues of the single-scattering properties related to the combined snow grains and BC/dust system.

1. We showed that for a given shape (four shapes are presented), the internal mixing case absorbs more light than the external mixing counterpart.
2. We illustrated that the effect of snow grain shape on the single-scattering albedo is relatively small; however, its effect on the asymmetry factor is substantial given the degree to which *g* is dependent on the complexity of snow grains. Compared to spheres, which have the strongest forward scattering, the volume-equivalent Koch snowflakes scatter much less, followed by plates and spheroids. Asymmetry factor differences between spheres and snowflakes defined by volume-equivalent radii of 100 μm are about 15% regardless of BC/dust concentration.
3. We demonstrated that, due to a greater probability of intercepting incoming photons, multiple inclusions of BC/dust particles produced by a stochastic process in snow grains exhibit a larger single-scattering coalbedo compared to a single inclusion having the same volume.
4. Using a Koch snowflake as an example, we found that internal mixture involving an aggregate absorbs more than the equal-volume spherical counterpart due to its ability to absorb and reflect more incident photons.
5. Calculations of the spectral single-scattering coalbedo, covering the 0.2–5 μm wavelength region, for snow grains composed of internal mixed BC/dust particles revealed that their effect on absorption is confined to wavelengths shorter than about 1.4 μm, beyond which ice absorption predominates. The asymmetry factor for snow grains is essentially independent of BC/dust absorption and exhibits a remarkable peak with a value close to 1 located at 2.85 μm, referred to as the Christiansen effect, where the extinction efficiency displays a strong max-min fluctuation around 2.

In summary, we have demonstrated the importance of multiple inclusions of internally mixed BC/dust in snow grains of various shapes in determining the single-scattering properties (extinction coefficient, single-scattering albedo, and asymmetry factor) of the combined BC/dust and snow system, which are required inputs to a radiative transfer model for radiative flux calculations.

We further studied the snow albedo reduction associated with BC/dust mixing states in snow grains using the single-scattering properties determined from stochastic and light absorption parameterizations developed in this work and employing the adding/doubling method for spectral radiative transfer.

©2014. American Geophysical Union. All Rights Reserved.

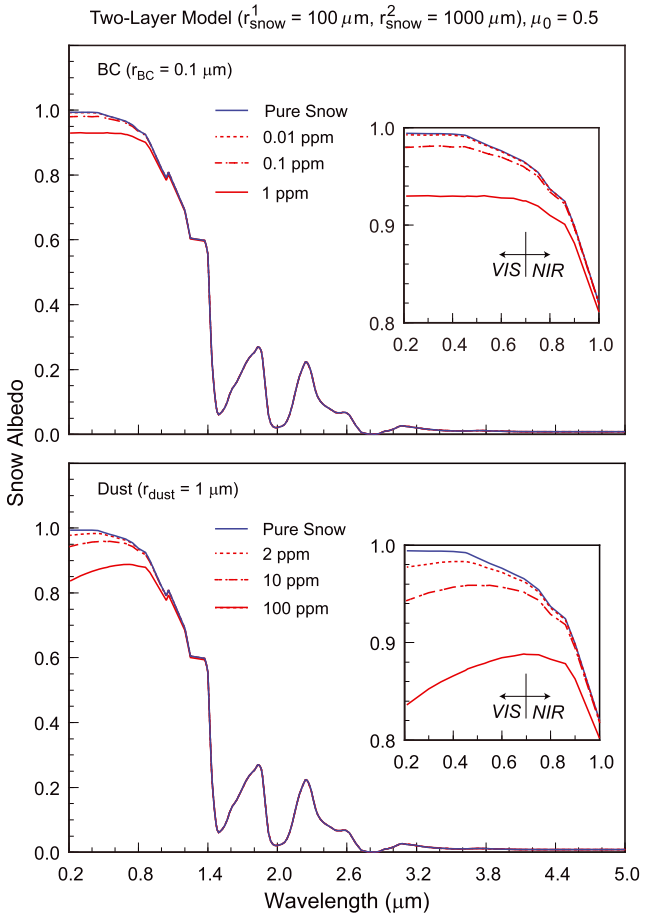

Figure 10. Snow albedo for a two-snow layer (new snow on top of old snow) as a function of wavelength for three BC/dust concentrations using the single-scattering properties depicted in Figure 6. The new snow internally mixed with (top) BC or (bottom) dust has an optical depth of 200, while the pure old snow is considered to be semiinfinite. The enlarged diagrams display snow albedo in the wavelength region 0.2–1 μm where substantial BC/dust absorption occurs.

1. Based on a combination of Koch snowflakes and internal/external mixed BC/dust particles as a prototype, we illustrated that visible snow albedo decreases with increasing BC/dust concentrations and that the internal mixing case reduces more than its external mixing counterpart.
2. Through the asymmetry factor, which is independent of the BC/dust mixing state, the snow grain shape plays a critical role in visible snow albedo calculations. Due to their relatively weak forward scattering, Koch snowflakes reflect more light than the spherical shape with spheroid and plate shapes in between the two.
3. We showed that visible snow albedo reduces more in the case of multiple inclusion of BC (or dust) spheres than that of an equal-volume single sphere, the degree of which is dependent on snow grain shape and a function of BC concentration.

Finally, we have constructed a two-layer spectral snow model covering the entire solar spectrum composed of contaminated fresh snow on top of pure old snow for application to land/snow models to study and understand the climatic impact of multiple internal mixing states of BC/dust associated with snow grain metamorphism, particularly over mountains/snow topography. Additionally, the single-scattering properties of four snow grain shapes (Koch snowflake, plate/column, spheroid, and sphere) coupled with a number of BC/dust mixing states might be useful to researchers who are conducting studies involving BC/dust and snow interaction and feedback in climate models. These advances in light scattering/absorption modeling for BC/dust-snow system would alleviate some of the uncertainties in radiative forcing analysis. Additional work is required to quantify uncertain reduction, however. Finally, we submit that the deposition of absorbing BC/dust aerosols onto the snow and glaciers over numerous majestic mountains (e.g., Tibetan Plateau) is a critical issue in the reduction of snow albedo vis-a-vis aerosols-mountain snow-albedo feedback that would have an irreversible impact on regional climate and climate change and available water resources.

Acknowledgments
This research was supported by the Department of Energy under grant DESC0006742, by the National Science Foundation under grant AGS-0946315, and by subcontract S100097 from the Texas A&M Research Foundation, which is sponsored by NASA under grant NNX11AK39G. Users can access the data from this paper via the authors without any restrictions.

References

Aoki, T., T. Aoki, M. Fukabori, A. Hachikubo, Y. Tachibana, and F. Nishio (2000), Effects of snow physical parameters on spectral albedo and bidirectional reflectance of snow surface, *J. Geophys. Res.*, *105*, 10,219–10,236, doi:10.1029/1999JD901122.

Aoki, T., K. Kuchiki, M. Niwano, Y. Kodama, M. Hosaka, and T. Tanaka (2011), Physically based snow albedo model for calculating broadband albedos and the solar heating profile in snowpack for general circulation models, *J. Geophys. Res.*, *116*, D11114, doi:10.1029/2010JD015507.

Borghese, F., P. Denti, R. Saija, and O. I. Sindoni (1992), Optical properties of spheres containing a spherical eccentric inclusion, *J. Opt. Soc. Am. A*, *9*, 1327–1335.

Born, M., and E. Wolf (1975), *Principles of Optics*, Pergamon, Oxford.

Christiansen, C. (1884), Untersuchungen über die optischen Eigenschaften von fein verteilten Körpern, *Ann. Phys. Chem.*, *23*, 298–306.

©2014. American Geophysical Union. All Rights Reserved.

Christiansen, C. (1885), Untersuchungen über die optischen Eigenschaften von fein verteilten Körpern, *Ann. Phys. Chem.*, *24*, 439–446.
Chýlek, P., V. Ramaswamy, and R. J. Cheng (1984), Effect of graphitic carbon on the albedo of clouds, *J. Atmos. Sci.*, *41*, 3076–3084.
d'Almeida, G. A., P. Koepke, and E. P. Shettle (1991), *Atmospheric Aerosols*, A. Deepak, Hampton, Va.
Doherty, S. J., S. G. Warren, T. C. Grenfell, A. D. Clarke, and R. E. Brandt (2010), Light-absorbing impurities in Arctic snow, *Atmos. Chem. Phys.*, *10*, 11,647–11,680.
Dominé, F., T. Lauzier, A. Cabanes, L. Legagneux, W. F. Kuhs, K. Techmer, and T. Heinrichs (2003), Snow metamorphism as revealed by scanning electron microscopy, *Micros. Res. Tech.*, *62*, 33–48.
Flanner, M. G., and C. S. Zender (2006), Linking snowpack microphysics and albedo evolution, *J. Geophys. Res.*, *111*, D12208, doi:10.1029/2005JD006834.
Flanner, M. G., X. Liu, C. Zhou, J. E. Penner, and C. Jiao (2012), Enhanced solar energy absorption by internally-mixed black carbon in snow grains, *Atmos. Chem. Phys.*, *12*, 4699–4721.
Friedlander, S. K. (2000), *Smoke, Dust, and Haze, Fundamentals of Aerosol Dynamics*, 2nd ed., Oxford Univ. Press, New York.
Fuller, K. A. (1995), Scattering and absorption cross sections of compounded spheres. III. Spheres containing arbitrarily located spherical inhomogeneities, *J. Opt. Soc. Am. A*, *12*, 893–904.
Garrett, T. J., H. Gerber, D. G. Baumgardner, C. H. Twohy, and E. M. Weinstock (2003), Small, highly reflective ice crystals in low-latitude cirrus, *Geophys. Res. Lett.*, *30*(21), 2132, doi:10.1029/2003GL018153.
Gerber, H., Y. Takano, T. Garrett, and P. V. Hobbs (2000), Nephelometer measurement of the asymmetry parameter, volume extinction coefficient and backscatter ratio in arctic clouds, *J. Atmos. Sci.*, *57*, 3021–3034.
Grenfell, T. C., S. G. Warren, and P. C. Mullen (1994), Reflection of solar radiation by the Antarctic snow surface at ultraviolet, visible, and near-infrared wavelengths, *J. Geophys. Res.*, *99*, 18,669–18,684, doi:10.1029/94JD01484.
Grenfell, T. C., S. J. Doherty, A. D. Clarke, and S. G. Warren (2011), Light absorption from particulate impurities in snow and ice determined by spectrophotometric analysis of filters, *Appl. Opt.*, *50*, 2037–2048.
Hadley, O. L., C. E. Corrigan, T. W. Kirchstetter, S. S. Cliff, and V. Ramanathan (2010), Measured black carbon deposition on the Sierra Nevada snow pack and implication for snow pack retreat, *Atmos. Chem. Phys.*, *10*(15), 7505–7513, doi:10.5194/acp-10-7505-2010.
Hammer, C. U., H. B. Clausen, W. Dansgaard, A. Neftel, P. Kristinsdottir, and E. Jonhson (1985), Continuous impurity analysis along the Dye 3 deep core, in *Greenland Ice Core: Geophysics, Geochemistry and the Environment*, *Geophys. Monogr.*, vol. 33, edited by C. C. Langway Jr., H. Oeschger, and W. Dansgaard, pp. 90–94, AGU, Washington, D. C.
Irvine, W. M., and J. B. Pollack (1968), Infrared optical properties of water and ice spheres, *Icarus*, *8*, 324–360.
Jacobson, M. Z. (2004), Climate response of fossil fuel and biofuel soot, accounting for soot's feedback to snow and sea ice albedo and emissivity, *J. Geophys. Res.*, *109*, D21201, doi:10.1029/2004JD004945.
Jacobson, M. Z. (2006), Effects of externally-through-internally-mixed soot inclusions within clouds and precipitation on global climate, *J. Phys. Chem. A*, *110*, 6860–6873.
Jacobson, M. Z. (2012), Investigating cloud absorption effects: Global absorption properties of black carbon, tar balls, and soil dust in clouds and aerosols, *J. Geophys. Res.*, *117*, D06205, doi:10.1029/2011JD017218.
Jenk, T. M., S. Szidat, M. Schwikowski, H. W. Gaggeler, S. Brutsch, L. Wacker, H. A. Synal, and M. Saurer (2006), Radiocarbon analysis in an Alpine ice core: Record of anthropogenic and biogenic contributions to carbonaceous aerosols in the past (1650–1940), *Atmos. Chem. Phys.*, *6*, 5381–5390.
Kang, S. C., Y. L. Zhang, Y. J. Zhang, B. Grigholm, S. Kaspari, D. H. Qin, J. W. Ren, and P. Mayewski (2010), Variability of atmospheric dust loading over the central Tibetan Plateau based on ice core glaciochemistry, *Atmos. Environ.*, *44*(25), 2980–2989, doi:10.1016/j.atmosenv.2010.05.014.
Krekov, G. M. (1993), Models of atmospheric aerosols, in *Aerosol Effects on Climate*, edited by S. G. Jennings, pp. 9–72, Univ. of Arizona Press, Tucson, Ariz.
Kumai, M. (1977), Electron microscope analysis of aerosols in snow and deep ice cores from Greenland, in *Isotopes and Impurities in Snow and Ice*, pp. 341–350, International Association of Hydrological Sciences, Grenoble.
Liou, K. N. (2002), *An Introduction to Atmospheric Radiation*, 2nd ed., Academic Press, San Diego, Calif.
Liou, K. N., Y. Takano, and P. Yang (2010), On geometric optics and surface waves for light scattering by spheres, *J. Quant. Spectrosc. Radiat. Transfer*, *111*, 1980–1989.
Liou, K. N., Y. Takano, and P. Yang (2011), Light absorption and scattering by aggregates: Application to black carbon and snow grain, *J. Quant. Spectrosc. Radiat. Transfer*, *112*, 1581–1594.
Liou, K. N., Y. Takano, Q. Yue, and P. Yang (2013), On the radiative forcing of contrail cirrus contaminated by black carbon, *Geophys. Res. Lett.*, *40*, 778–784, doi:10.1002/grl.50110.
Macke, A., M. I. Mishchenko, and B. Cairns (1996), The influence of inclusions on light scattering by large ice particles, *J. Geophys. Res.*, *101*, 23,311–23,316, doi:10.1029/96JD02364.
Ming, J., H. Cachier, C. Xiao, D. Qin, S. Kang, S. Hou, and J. Xu (2008), Black carbon record based on a shallow Himalayan ice core and its climatic implications, *Atmos. Chem. Phys.*, *8*, 1343–1352.
Ming, J., C. Xiao, H. Cachier, D. Qin, X. Qin, Z. Li, and J. Pu (2009), Black carbon (BC) in the snow of glaciers in west China and its potential effects on albedos, *Atmos. Res.*, *92*, 114–123.
Petzold, A., J. Ström, S. Ohlsson, and F. P. Schröder (1998), Elemental composition and morphology of ice-crystal residual particles in cirrus clouds and contrails, *Atmos. Res.*, *49*, 21–34.
Petzold, A., A. Döpelheuer, C. A. Brock, and F. P. Schröder (1999), In situ observations and model calculations of black carbon emission by aircraft at cruise altitude, *J. Geophys. Res.*, *104*, 22,171–22,181, doi:10.1029/1999JD900460.
Schwarz, J. P., R. S. Gao, A. E. Perring, J. R. Spackman, and D. W. Fahey (2013), Black carbon aerosol size in snow, *Sci. Rep.*, *3*, 1356–1360, doi:10.1038/srep01356.
Sterle, K. M., J. R. McConnell, J. Dozier, R. Edwards, and M. G. Flanner (2013), Retention and radiative forcing of black carbon in eastern Sierra Nevada snow, *Cryosphere*, *7*(1), 365–374, doi:10.5194/tc-7-365-2013.
Takano, Y., and K. N. Liou (1989), Solar radiative transfer in cirrus clouds. Part I. Single-scattering and optical properties of hexagonal ice crystals, *J. Atmos. Sci.*, *46*, 3–19.
Takano, Y., and K. N. Liou (1995), Radiative transfer in cirrus clouds. Part III: Light scattering by irregular ice crystals, *J. Atmos. Sci.*, *52*, 818–837.
Takano, Y., K. N. Liou, and P. Yang (2012), Diffraction by rectangular parallelepiped, hexagonal cylinder, and three-axis ellipsoid: Some analytic solutions and numerical results, *J. Quant. Spectrosc. Radiat. Transfer*, *113*, 1836–1843.
Takano, Y., K. N. Liou, M. Kahnert, and P. Yang (2013), The single-scattering properties of black carbon aggregates determined from the geometric-optics surface-wave approach and the T-matrix method, *J. Quant. Spectrosc. Radiat. Transfer*, *125*, 51–56.
Thevenon, F., F. S. Anselmetti, S. M. Bernasconi, and M. Schwikowski (2009), Mineral dust and elemental black carbon records from an Alpine ice core (Colle Gnifetti glacier) over the last millennium, *J. Geophys. Res.*, *114*, D17102, doi:10.1029/2008JD011490.

©2014. American Geophysical Union. All Rights Reserved.

Videen, G., and P. Chýlek (1998), Scattering by a composite sphere with an absorbing inclusion and effective medium approximations, *Opt. Commun.*, *158*, 1–6.

von Koch, H. (1904), Sur une courbe continue sans tangente, obtenue par une construction géométrique élémentaire, *Ark. Mat.*, *1*, 681–704.

Warren, S. G., and R. E. Brandt (2008), Optical constants of ice from the ultraviolet to the microwave: A revised compilation, *J. Geophys. Res.*, *113*, D14220, doi:10.1029/2007JD009744.

Warren, S. G., and W. J. Wiscombe (1980), A model for the spectral albedo of snow. II: Snow containing atmospheric aerosols, *J. Atmos. Sci.*, *37*, 2734–2745.

Wiscombe, W. J., and S. G. Warren (1980), A model for the spectral albedo of snow: I. Pure snow, *J. Atmos. Sci.*, *37*, 2712–2733.

Xu, B., et al. (2009), Black soot and the survival of Tibetan glaciers, *Proc. Natl. Acad. Sci. U.S.A.*, *106*, 22,114–22,118.

Yang, P., and K. N. Liou (1997), Light scattering by hexagonal ice crystals: Solutions by a ray-by-ray integration algorithm, *J. Opt. Soc. Am. A*, *14*, 2278–2289.

Yang, P., L. Bi, B. Baum, K. N. Liou, G. Kattawar, M. Mishchenko, and B. Cole (2013), Spectrally consistent scattering, absorption, and polarization properties of atmospheric ice crystals at wavelengths from 0.2 to 100 μm, *J. Atmos. Sci.*, *70*, 330–347.

Zdanowicz, C. M., G. A. Zielinski, and C. P. Wake (1998), Characteristics of modern atmospheric dust deposition in snow on the Penny Ice Cap, Baffin Island, Arctic Canada, *Tellus*, *50B*, 506–520.

Zdanowicz, C., G. Hall, J. Vaive, Y. Amelin, J. Percival, I. Girard, P. Biscaye, and A. Bory (2006), Asian dustfall in the St. Elias Mountains, Yukon, Canada, *Geochim. Cosmochim. Acta*, *70*, 3493–3507.

©2014. American Geophysical Union. All Rights Reserved.